Chapter 2
Axial Capillary Forces

Pierre Lambert and Jean-Baptiste Valsamis

Abstract This chapter presents classical techniques to compute the shape of a meniscus using the energetic method and its numerical implementation using Surface Evolver. It provides the numerical solution of the Laplace equation for axially symmetric configuration and some useful analytical approximations (circular or toroidal approximation, parabolic approximation). Formal equivalence between these approaches is given and results are provided as rules of thumbs for the designer.

2.1 Introduction

The contribution of this chapter is to model the force exerted on solids by capillary bridges. These liquid bridges can be seen as mechanical joints with 6 degrees-of-freedom. This chapter focuses on the axial degree of freedom, i.e. on the forces developed along the symmetry axis of the liquid bridges.

As experimentally confirmed in the previous chapter (as shown in Fig. 1.1), the very first model of a phenomenon usually relies on its scaling law, acknowledging in this case the linear dependence of capillary forces on the size of the set up, and more generally, the importance of dimensional analysis and scaling laws.

Nevertheless, targeting the design of devices using surface tension effects, it is useful to get a more detailed insight on the parameters ruling capillary forces. This is the starting point of models development. The axial capillary forces are of interest in all micromanipulation case studies, to know for example the amount of picking force in a microassembly application. At the nanoscale, the capillary force is an

P. Lambert (✉) · J.-B. Valsamis
BEAMS Department, Université libre de Bruxelles, CP 165/56,
Avenue F.D. Roosevelt, 50, 1050 Brussels, Belgium
e-mail: pierre.lambert@ulb.ac.be

J.-B. Valsamis
e-mail: jvalsami@ulb.ac.be

P. Lambert (ed.), *Surface Tension in Microsystems*, Microtechnology and MEMS,
DOI: 10.1007/978-3-642-37552-1_2, © Springer-Verlag Berlin Heidelberg 2013

important contribution to adhesion, such as for example adhesion in atomic force microscopy or stiction in RF MEMS. The lateral capillary forces models are more dedicated to self-assembly problems or to the dynamics of components floating on solder paste menisci, such as in flip-chip assembly. The dynamics of a chip in contact with a fluid meniscus has been studied as a classical second order system, including inertial, viscous and stiffness effects. Only the stiffness term depends on capillary forces, while the viscous term depends on the shear stress on the component, i.e. on the liquid viscosity and the liquid flow inside the meniscus.

In order to make our results useful to readership we try to propose analytical models or to present numerical results in the form of maps and graphs.

2.2 Modeling Liquid Bridges Geometry: An Overview

Literature highlights two different ways to compute capillary forces. The first one consists in computing first the surface energy of the liquid bridge and deriving it with respect to the degree-of-freedom of interest[1] (see Sect. 2.2.1). This approach is particularly well suited for systems smaller than the capillary length, because in this case, gravity energy and inertial effects are typically smaller than surface energy. The second approach directly gives the force from the liquid bridge geometry (Sect. 2.2.3). Note that in both cases finding the right liquid bridge geometry is the key point, leading to some useful approximations (Sect. 2.2.4). Computing the force from surface energy is quite straightforward and will be done in the following. On the contrary, beside this approach based on energy, a second approach based on forces directly was highlighted in literature: basically, it consists in computing separately the effect of surface tension and the effect of pressure gap induced by the curvature of the liquid bridge. We contributed to that point by giving formal and experimental evidences of the equivalence of both approaches [1]. This will be detailed later on in Sect. 2.4. Consequently, in the current section, we don't focus on force computation but rather on liquid bridge geometry. The link between geometry and force will be introduced later on.

Additional details can be found in our related publications [1–3].

2.2.1 Energetic Method: Example of Two Parallel Plates

As an introduction, we propose the case of a meniscus between two parallel plates, with a contact angle $\theta = \pi/2$. This method consists in:

- writing the interfacial energy W of the system as a function of the parameters defining the geometry of the system;

[1] E.g. the force along the z-direction is the derivative of the energy with respect to z.

- deriving this energy with respect to one of the parameters (the separation distance z is often used) in order to calculate the capillary force as a function of this parameter;
- estimating the derivative of the other parameters with respect to the chosen parameter by assuming a mathematical relationship (for example the conservation of the liquid volume).

This approach can be illustrated by the case of two parallel plates linked by a meniscus, such as represented in Fig. 2.1:

The system has three phases (S: solid, L: liquid, V: vapor) and three interfaces (LV:liquid–vapor, SL: solid–liquid, SV: solid–vapor) leading to a total energy equal to:

$$W = W_{SL} + W_{SV} + W_{LV} = \gamma_{SL} S_{SL} + \gamma_{SV} S_{SV} + \gamma \Sigma \tag{2.1}$$

where:

$$W_{SL} = 2\gamma_{SL}\pi r^2 \tag{2.2}$$
$$W_{SV} = 2\gamma_{SV}(\pi r_0^2 - \pi r^2) \tag{2.3}$$
$$W_{LV} = \gamma \Sigma = \gamma 2\pi r z \tag{2.4}$$

In these equations, r_0 is an arbitrary constant radius, larger than r and $\gamma_{SL}(\gamma_{SV})$ represents the interfacial energy between solid and the liquid (vapor). Σ represents the area of the liquid-vapor interface (the lateral area of the meniscus). This leads to:

$$\begin{aligned} W &= 2\gamma_{SL}\pi r^2 + 2\gamma_{SV}(\pi r_0^2 - \pi r^2) + \gamma 2\pi r z \\ &= \underbrace{2\gamma_{SV}\pi r_0^2}_{\text{constant}} - 2\pi r^2 \underbrace{(\gamma_{SV} - \gamma_{SL})}_{\gamma\cos\theta = 0} + \gamma 2\pi r z \end{aligned}$$

As we try to get the expression of the force F acting on one of the plates along the vertical axis z as a function of the separation distance z, the latter equation must be derived with respect to z:

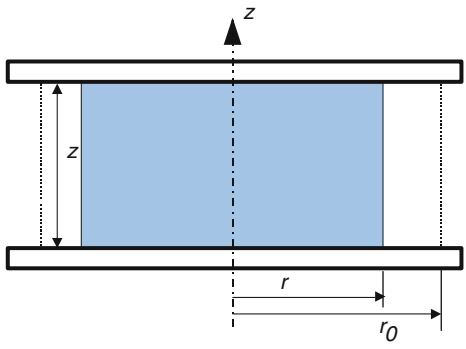

Fig. 2.1 Example of the energetic method: case of two parallel plates. z is the gap between plates, r the wetting radius i.e. the radius of the wetting circle, and r_0 an arbitrary radius for area computation (see the related explanation in the text)

$$F = -\frac{\mathrm{d}W}{\mathrm{d}z}$$
$$= -2\pi r\gamma - \underbrace{2\pi z\gamma\frac{\mathrm{d}r}{\mathrm{d}z}}_{\text{requires an additional assumption}} \tag{2.5}$$

In order to calculate all the derivatives involved in this expression, an additional assumption must be stated. The assumption is that the volume $V = \pi r^2 z$ of the meniscus remains constant (we consequently do not consider the evaporation of the liquid), and its conservation leads to:

$$\frac{\mathrm{d}V}{\mathrm{d}z} = 2\pi rz\frac{\mathrm{d}r}{\mathrm{d}z} + \pi r^2 = 0 \tag{2.6}$$

Finally, combining both latter equations, the force can be written as:

$$F = -\pi r\gamma \tag{2.7}$$

Of course, this method only gives an exact analytical result in the very restrictive case of two parallel plates and a contact angle equal to $\pi/2$. When the liquid-vapor interface cannot be estimated analytically, it is necessary to turn oneself toward a software such as Surface Evolver (see next section).

Israelachvili [4] applied this method to calculate the capillary force between a sphere and a flat surface[2]:

$$F = -4\pi R\gamma\cos\theta \tag{2.8}$$

where R is the sphere radius, γ is the surface tension, and $\cos\theta$ the mean cosine of contact angles θ_1 and θ_2 on sphere and plate respectively.

Let us add a recently published model [6] giving an analytical expression for the capillary force between two spheres with radii R_1 and R_2, as a function of the separation distance z:

$$F_{\text{sphere/sphere}} = -\frac{2R\cos\theta}{1 + z/(2h)} \tag{2.9}$$

where R is the equivalent radius given by $R = \frac{2R_1R_2}{R_1+R_2}$, $2\cos\theta = \cos\theta_1 + \cos\theta_2$, z is the separation distance or gap and h is the immersion height, approximately given by [6]:

$$h = \frac{z}{2}\left(-1 + \sqrt{1 + 2V/(Rz^2)}\right) \tag{2.10}$$

where V is the volume of the liquid bridge.

[2] As it can be seen this expression does not depend on the volume of liquid. This approximation is only valid for small volumes. More rigorous expressions, valid for large volumes are given by [5].

2.2.2 Introduction to Surface Evolver

Surface Evolver is a simulation software which computes minimal energy surfaces.[3] Therefore, in this software, constraints on contact angles, pinning lines, volume of liquid must be defined in a text file which is processed to evolve the vapor-liquid interface toward an energy minimum (Fig. 2.2).

In general, the energy can be written as (see previous section):

$$W = \text{constant} - \underbrace{A_{SL}\underbrace{(\gamma_{SV} - \gamma_{SL})}_{\gamma\cos\theta}}_{I} + \gamma\Sigma \tag{2.11}$$

The surface energy $\gamma\Sigma$ is easy to compute as soon as the liquid-vapor is meshed. But usually in Surface Evolver, what is meshed is **only** this surface and **not** the solid-liquid interface (Fig. 2.3).

Therefore, the energetic content of this interface $-A_{SL}\gamma\cos\theta$ has to be computed from the single elements of this interface to be meshed, which in this case is its boundary, i.e. the triple line. This is achieved using the Stokes theorem:

$$\iint \text{rot}\bar{w}\cdot \mathrm{d}\bar{S} = \oint \bar{w}\cdot \mathrm{d}\bar{l} \tag{2.12}$$

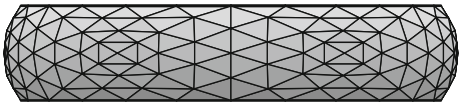

Fig. 2.2 Example of a meniscus meshed in surface evolver

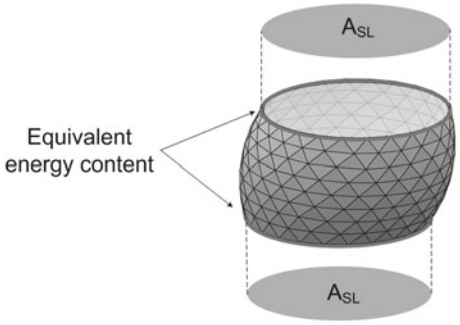

Fig. 2.3 The surface energy of the meniscus must be computed from the meshed elements, i.e. from the triple line

[3] Available at http://www.susqu.edu/brakke/evolver/evolver.html.

where rot$\bar{w}$ is equal to $\bar{\nabla} \times \bar{w}$:

$$\begin{aligned}\bar{\nabla} \times \bar{w} =&(\partial_y w_z - \partial_z w_y)\bar{1}_x + (\partial_x w_z - \partial_z w_x)\bar{1}_y ... \\ &... + (\partial_x w_y - \partial_y w_y)\bar{1}_z \qquad (2.13)\\ =&\left(\frac{1}{r}\partial_\theta w_z - \partial_z w_\theta\right)\bar{1}_r + (\partial_z w_r - \partial_r w_z)\bar{1}_\theta ... \\ &... + \frac{1}{r}(\partial_r (r w_\theta) - \partial_\theta w_r)\bar{1}_z \qquad (2.14)\end{aligned}$$

The integral I defined in (2.11) can be developed using $\bar{\nabla} \times \bar{w} = \bar{1}_z$:

$$I = -2\gamma \cos\theta \underbrace{\iint \bar{1}_z \cdot \mathrm{d}\bar{S}}_{A_{SL}} = -2\gamma \cos\theta \oint \bar{w} \cdot \mathrm{d}\bar{l} \qquad (2.15)$$

with:

$$\bar{w} = x\bar{1}_y = r \sin\theta \cos\theta \bar{1}_r + r \cos^2\theta \bar{1}_\theta \qquad (2.16)$$

and:

$$\mathrm{d}\bar{l} = r\mathrm{d}\theta \bar{1}_\theta \qquad (2.17)$$

The vector $\bar{w}$ must be defined in the input file of Surface Evolver, so that the software can compute the energetical content of the non-meshed interface.

Similarly, we saw in the previous section that the condition of constant volume was imposed to achieve the computation. Here again, Surface Evolver needs information to compute a volume V of which only a part of its boundary is meshed. We refer now to the divergence theorem (Fig. 2.4):

$$\iiint_V \int \mathrm{div}\bar{u}\mathrm{d}V = \oiint_{\partial V} \bar{u} \cdot \mathrm{d}\bar{S} \qquad (2.18)$$

Choosing a vector $\bar{u}$ whose divergence is equal to 1, the volume can be written as:

$$V = \iiint_V \mathrm{d}V$$

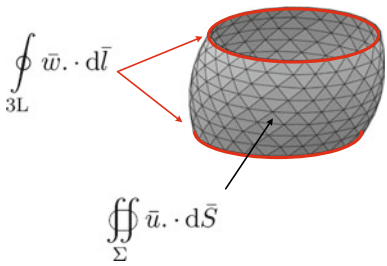

Fig. 2.4 The volume of the meniscus must be computed from the meshed elements, i.e. by summing a contribution from the lateral area Σ and a contribution from the triple line (3L)

$$= \iint_{\Sigma} \bar{u}. \cdot \mathrm{d}\bar{S} + \iint_{\mathrm{SL}} \underbrace{\bar{u}}_{\mathrm{rot}\bar{w}} . \cdot \mathrm{d}\bar{S}$$

$$= \iint_{\Sigma} \bar{u}. \cdot \mathrm{d}\bar{S} + \oint_{\mathrm{3L}} \bar{w}. \cdot \mathrm{d}\bar{l} \tag{2.19}$$

where Σ denotes the meshed liquid-vapor interface, SL the solid-vapor interface (not meshed) and 3L the triple line contours (on top and bottom of the meniscus). The vector $\bar{w}$ is defined by $\mathrm{rot}\bar{w} = z(x, y)\bar{1}_z$ where $z(x, y)$ is the equation of the solid-liquid interface.

Example: Truncated Cone

Let us take the case of a truncated cone limited by the planes $z = 0$ and $z = z_H$ (such as depicted in Fig. 2.5). The cone equation is:

$$r(z) = r_H + (z_H - z)\tan a \tag{2.20}$$

and the normal vector is given by:

$$\bar{n} = \cos a\,\bar{1}_r + \sin a\,\bar{1}_z \tag{2.21}$$

With the surface element $\mathrm{d}S = \frac{r}{\cos a} dz d\theta$, the volume is computed as follows:

$$V = \iint_{\Sigma} z\bar{1}_z. \cdot \mathrm{d}\bar{S} + \oint_{\mathrm{3L}} \bar{w}. \cdot \mathrm{d}\bar{l}$$

$$= \iint_{\Sigma} z\bar{1}_z. \cdot \mathrm{d}\bar{S} + \oint_{\mathrm{3L}} z_H r_H \cos\theta(\sin\theta\bar{1}_r + \cos\theta\bar{1}_\theta) \cdot r_H \mathrm{d}\theta\bar{1}_\theta$$

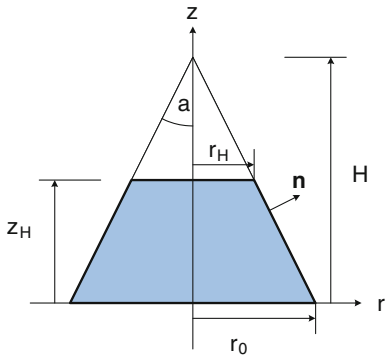

Fig. 2.5 Truncated cone illustrating the computation of volume is surface evolver

$$= \int_0^{2\pi} \mathrm{d}\theta \int_0^{z_H} \tan a\, r(z) z \mathrm{d}z + z_H r_H^2 \int_0^{2\pi} \cos^2\theta \mathrm{d}\theta$$
$$= \pi r_H z_H^2 \tan a + \frac{\pi}{3} z_H^3 \tan^2 a + \pi r_H^2 z_H \tag{2.22}$$

which is obviously equal to the difference of two cone volumes ($r_0 = r(z=0)$)*:*

$$V = \frac{\pi}{3} r_0^2 H - \frac{\pi}{3} r_H^2 (H - z_H) \tag{2.23}$$

Surface Evolver has been used to deduce lateral capillary forces and capillary forces due to capillary condensation [7].

2.2.3 Exact Resolution for Axially Symmetric Problems

For axially symmetric menisci of equation $r = r(z)$, the curvature $2H$ can be written as follows (see [3] for details):

$$2H = -\frac{r''}{(1+r'^2)^{\frac{3}{2}}} + \frac{1}{(1+r'^2)^{\frac{1}{2}}} = \frac{p_{\text{in}} - p_{\text{out}}}{\gamma} \equiv \frac{\Delta p}{\gamma} \tag{2.24}$$

where p_{in} and p_{out} are the pressures inside and outside the liquid bridge, and γ is the surface tension of the considered liquid. Δp is the pressure gap across the liquid-gas interface: as it will be seen later on, it is one of the drivers of capillary forces. This equation was first derived by Pierre-Simon Laplace in 1805 [8] (Fig. 2.6).

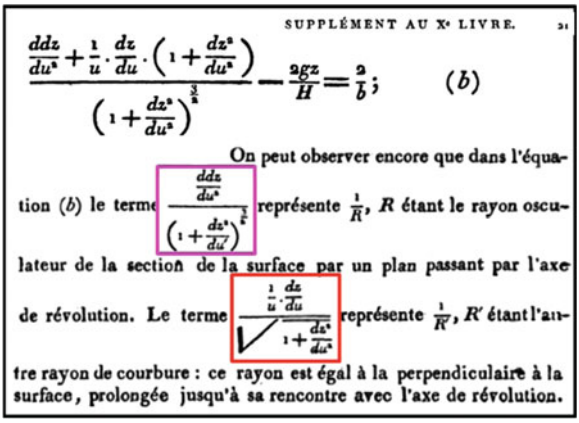
SUPPLÉMENT AU X^e LIVRE. 21

$$\frac{\frac{ddz}{du^2} + \frac{1}{u}\cdot\frac{dz}{du}\cdot\left(1+\frac{dz^2}{du^2}\right)}{\left(1+\frac{dz^2}{du^2}\right)^{\frac{3}{2}}} - \frac{2gz}{H} = \frac{2}{b}; \qquad (b)$$

On peut observer encore que dans l'équation (b) le terme $\frac{\frac{ddz}{du^2}}{\left(1+\frac{dz^2}{du^2}\right)^{\frac{3}{2}}}$ représente $\frac{1}{R}$, R étant le rayon osculateur de la section de la surface par un plan passant par l'axe de révolution. Le terme $\frac{\frac{1}{u}\cdot\frac{dz}{du}}{\sqrt{1+\frac{dz^2}{du^2}}}$ représente $\frac{1}{R'}$, R' étant l'autre rayon de courbure : ce rayon est égal à la perpendiculaire à la surface, prolongée jusqu'à sa rencontre avec l'axe de révolution.

Fig. 2.6 Laplace's original equation [8]

As illustrated in Fig. 2.7, it can be seen that the first term of (2.24) is the curvature of the planar curve defined by the meniscus profile, known to be $\frac{d\theta}{ds}$ where θ is the angle between the meniscus tangent and a fixed direction, for example the horizontal direction. ds is the infinitesimal intrinsic length along the meniscus. Consequently, the first curvature radius is $\frac{ds}{d\theta}$. The second curvature radius is the distance between the surface and the symmetry axis along the normal vector, given by $r/\sin\theta$.

Let us now put (2.24) as a system of two first-order differential equations:

$$\begin{cases} u = \frac{dr}{dz} \\ \frac{du}{dz} = \frac{1+u^2}{r} - \frac{\Delta p}{\gamma}(1+u^2)^{\frac{3}{2}} \end{cases} \tag{2.25}$$

To solve these equations, Δp must be known and boundary conditions have to be set (Fig. 2.8): let us assume that we know the point P of the meniscus in contact with the gripper. Therefore z_P and $r_P = r(z_P)$ are given by the initial coordinates of P and the slope of the meniscus in P is given by:

$$u_P = \frac{dr}{dz}|_{z_P} = \begin{cases} \frac{1}{\tan(\phi_P+\theta_2)}, & \text{if}(\theta_2+\phi_P) \neq \frac{\pi}{2} \\ 0, & \text{if}(\theta_2+\phi_P) = \frac{\pi}{2} \end{cases} \tag{2.26}$$

where the contact angle θ_2 and ϕ_P depends on the gripper geometry.

In our problem (how to determine the meniscus for given contact angles θ_1 and θ_2 and liquid volume V), only θ_2 is known. Indeed, Δp and the position of P are a priori

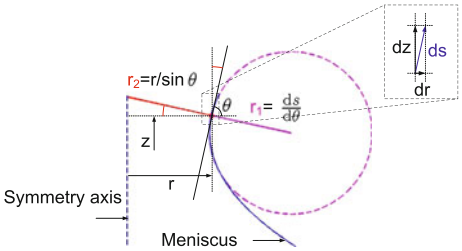

Fig. 2.7 Curvature radii of an axially symmetric surface: r_1 is the azimuthal curvature radius (in a plane containing the symmetry axis) and r_2 is the radial curvature radius (distance between the curve and the symmetry axis, measured along the normal)

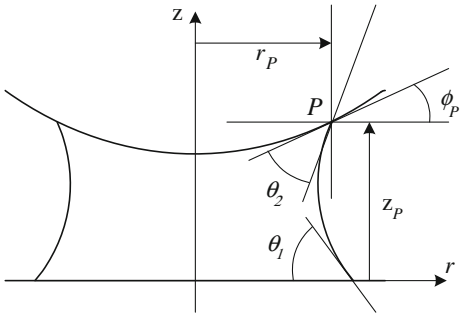

Fig. 2.8 Boundary conditions depend on the geometry and materials: the *upper line* states for the gripper, while the *lower straight line* states for the component

unknown. De Lazzer et al. [9] already suggested to iterate on Δp in order to adjust θ_1 to the prescribed value. Indeed, increasing pressure difference (i.e. more negative Δp) leads to a more curved meniscus, and, consequently, to smaller θ_1. P is still unknown and the condition on V has not yet been used. Therefore, a second iteration loop is used [10] to determine P: an initial position of P is guessed in order to solve the first iteration loop (i.e. determine a meniscus that would be correct as far as contact angles are concerned), leading to a candidate whose volume is computed. If this volume is smaller (larger) than the prescribed one, P is moved away (closer) from the symmetry axis (this is achieved by dichotomous search). This double iterative scheme is actually an application of the so-called shooting method. It is graphically illustrated in Fig. 2.9.

2.2.4 Geometrical Models

It has been seen in the previous section that solving (2.24) requires the knowledge of two initial values (position and slope of the meniscus) and the pressure difference parameter. Therefore, three conditions of the problem were used: the volume of liquid, the initial slope and the final slopes. These three conditions can alternatively be used to find the three parameters of a circle (two center coordinates and the radius) or the three coefficients of the parabola $r(z) = a_0 + a_1 z + a_2 z^2$ (Fig. 2.10).

These models are physically incorrect, but they provide a good estimate of the meniscus geometry from which the force is computed. Moreover, the parabolic model provides a full analytical resolution, as shown by Valsamis in his doctoral dissertation [11]. He also provided two maps (see Sect. 2.3.2.4) giving the relative error of these models with respect with the exact numerical resolution of (2.24).

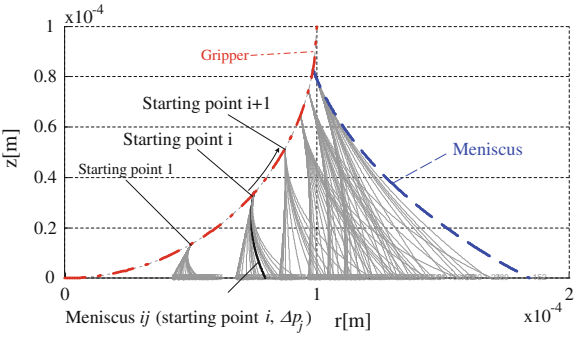

Fig. 2.9 Graphical illustration of the double iterative scheme for a sphere of 100 μm radius, contact angles equal to 3°, a volume of liquid equal to 45 nL and a gap equal to zero. Meniscus ij is obtained with the ith starting point and the jth pressure difference (Reprinted with permission from [1]. Copyright 2005 American Chemical Society)

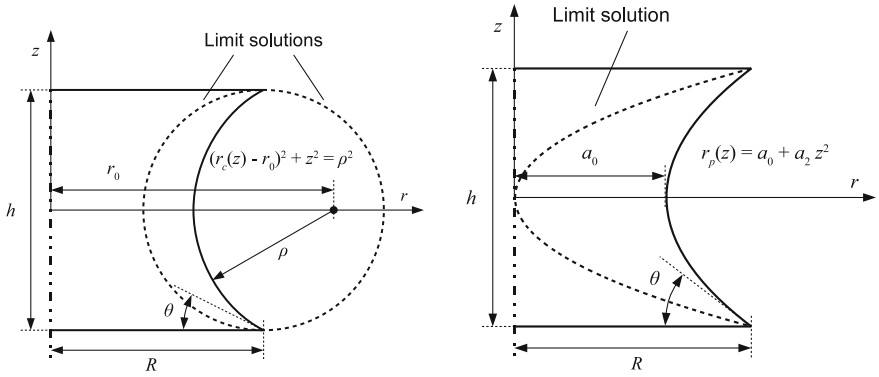

Fig. 2.10 Circular and parabolic models (Courtesy of J.-B. Valsamis [11])

As a conclusion, the meniscus shape may be assumed circular, which is valid when the radius r of the triple line is much larger than the meniscus height, or it may me assumed parabolic, which is valid for contact angles near $\pi/2$. The parabolic model has been used to get analytical estimates of the axial stiffness and in combination with gas law.

Remarks We have seen different methods to compute the geometry of a liquid bridge at equilibrium. When using surface energy minimization, the surface energy is known and the link to capillary force is obvious (the force is found by derivation). For both other methods, the link between geometry on the one hand and capillary force on the other hand has to be explained: this is the focus of next section.

2.3 Pinned and Non Pinned Triple Lines

The pinning of the triple line is made possible at the intersection between two surfaces with different surface energies or on sharp edges.

2.3.1 Non Pinned Menisci

The double iterative scheme briefly presented in Fig. 2.9 allowed us to study the influence of the pertinent parameters on the capillary forces between two solids: surface tension γ, contact angle θ, volume of liquid V, separation distance between both solids z. All these numerical experiments were performed with axial symmetry, solving (2.24).

Preliminarily, in order to validate the developed simulation code, we have studied the case of two parallel plates separated by a distance b and for a difference of pressure

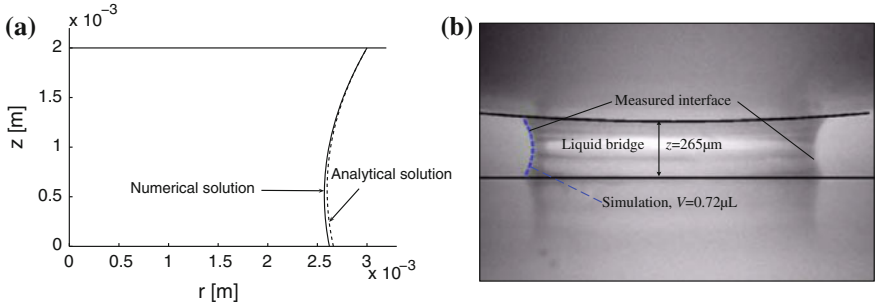

Fig. 2.11 Study of the meniscus shape **a** Comparison between the numerical and analytical meniscus shape, with $\Delta p = 0$, $a = 3\,\text{mm}$, $b = 2\,\text{mm}$ and $\theta_2 = 60°$; **b** Comparison between the simulation and the experimental meniscus shape (water, steel flat component, steel sphere ($R = 6.35\,\text{mm}$))(Reprinted with permission from [1]. Copyright 2005 American Chemical Society)

equal to zero, leading to the analytical equation of a catenary curve [3] (Fig. 2.11a). For $z = 0$, the relative error between the numerical radius and the analytical one is about 1.5 %.

A second case has been tested, namely the case of a meniscus between two parallel plates, with contact angles equal to 90°, leading to a cylindrical meniscus (with radius R) whose principal curvature radii are $R_1 = \infty$ and $R_2 = R$.

The last verification operated on the meniscus shape is the comparison between the output profile and the picture of the meniscus, as presented in Fig. 2.11b. This picture corresponds to a 12.7 mm diameter sphere linked to a steel component with 0.72 μL water. The gap in this case is 265 μm. The dashed line states for the meniscus output by the simulation tool.

The numerical computation of the force has also been compared with the analytical approximation (2.8) of the capillary force between a plane and a sphere (radius R), for a gap equal to zero and an equivalent contact angle $\theta\left(\text{if } \theta_1 \neq \theta_2, \cos\theta \equiv \dfrac{\cos\theta_1 + \cos\theta_2}{2}\right)$.

$$F = 4\pi R\gamma\cos\theta \tag{2.27}$$

Figure 2.12 plots the force as a function of the equivalent contact angle θ for a 26 mm diameter sphere and for two liquids: the upper curve shows the force for water and the lower one that for silicone oil (R47V50). It can be seen on this picture that the results of the simulations tend to the analytical approximations (solid and dashed lines).

After these preliminary validations, the influence of the following parameters was studied:

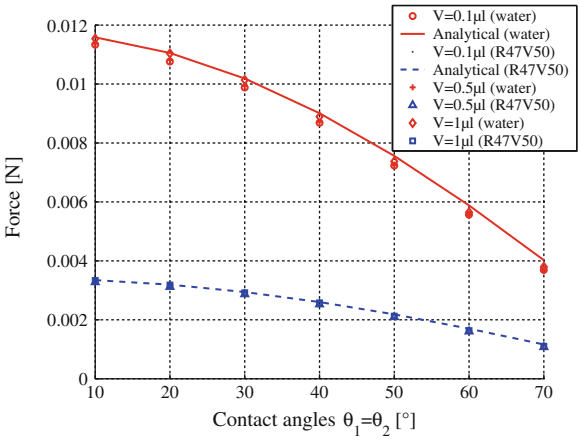

Fig. 2.12 Comparison between the simulation results and the analytical approximation $F = 4\pi\gamma R\cos\theta$ for a 13.0 mm diameter sphere, $\gamma = 72 \times 10^{-3}$ N m^{-1} (water) and $\gamma = 20.8 \times 10^{-3}$ N m^{-1} (silicone oil R47V50). The results are presented for different volumes (0.1, 0.5 and 1 µL) and different contact angles simulating different materials; the simulation points tend to the analytical approximations for water (*solid line*) and silicone oil (*dashed line*) (Reprinted with permission from [1]. Copyright 2005 American Chemical Society)

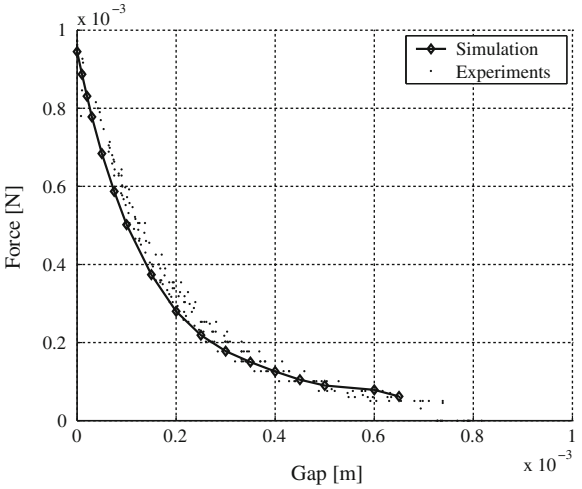

Fig. 2.13 Force-Distance curve for $V = 0.5$ µL R47V50, Si-component and GS-St-7.9 (Both reprinted with permission from [1]. Copyright 2005 American Chemical Society)

1. **Separation distance**: The curve of Fig. 2.13 plots the capillary force exerted by a 7.9 mm diameter sphere (see [3] for details) on a silicon component. The force is exerted by a 0.5 µL silicone oil droplet (R47V50). This curve has been measured with an almost zero velocity (equilibrium curve). As far as the simulation is concerned, receding contact angles have been input since the meniscus is stretched

by moving the sphere upwards. The correspondence between simulation and experiment can be seen on this picture although the rupture distance predicted by the simulation is a little smaller than the measured one.
This result indicates that the simulation tool can predict the capillary force with separation distances different from zero: this comes as a complement to the previous validations made by comparing the simulation with the analytical approximations, that was valid only at contact.

2. **Pressure term versus tension term**: The simulation results of Fig. 2.13 also allow to calculate and compare the importance of the interfacial tension force and the Laplace term of the capillary force (see Fig. 2.14). The results presented in this figure justify some approximations found in the literature, neglecting the 'tension' term for small gaps. Nevertheless, this assumption is no longer valid for larger gaps where the tension term even becomes dominant.
3. **Surface tension**: Additionally, the force has been shown to be proportional to surface tension γ which ranges from 20 to 72 mNm^{-1} for usual liquids such as alcohols, silicone oils or water. Solder pastes can exhibit surface tensions as high as a few hundreds of mNm^{-1}, leading to an important surface tension effect in solder paste assembly processes. An increase of surface tension nevertheless increases the contact angle (i.e. reduces the wettability), leading to a decrease of the force: the cut-off between both effects cannot be decided without numerical quantification.
4. **Volume of liquid**: The influence of the volume of liquid depends on the geometry of the objects. It can be surprising indeed in (2.8) to observe that the force does not depend on the volume of liquid. Hence this formula is widely used in capillary adhesion studies, since the exact volume of liquid got by capillary condensation

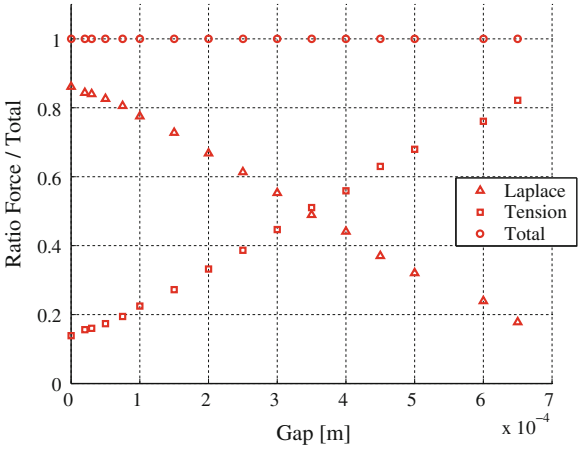

Fig. 2.14 Respective contribution of the 'tension' and 'Laplace' terms in the total amount of the force—Ratios without dimensions (Reprinted with permission from [1]. Copyright 2005 American Chemical Society)

is usually unknown. This formula is nevertheless only valid for small volumes of liquid (the so-called *immersion height* must be small). Other geometries lead to different dependences on the volume of liquid: for conical tips, the force increases with increasing volume of liquid.

As a conclusion of this part of the work, we set up a numerical tool ready to compute the force in whatever axially symmetric geometry. Three main limitations arise: (1) finding an optimum with a numerical tool is very tedious; (2) non axially symmetric geometries cannot be studied with this tool: the case of lateral capillary forces will be considered in Chap. 3; (3) finally, the dynamical aspects will be studied in Part III.

2.3.2 Pinned Menisci

2.3.2.1 Parabolic Model

As briefly exposed previously, we must distinguish between non-pinned menisci with imposed contact angle and pinned menisci with imposed wetting radius. In the latter case, such as depicted in Fig. 2.15, analytical approximations can be set, which is of the utmost interest to serve as benchmarks or to be exploited in design. According to Sect. 2.2.4 on geometrical approximations, it must be chosen between circular and parabolic models.

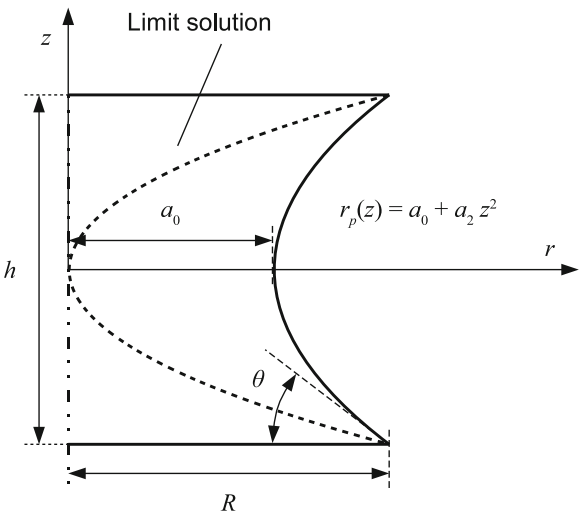

Fig. 2.15 Parabola model: as usual, three information (pinned contact angle, pad radius and gap) are used to determine the three coefficients of a parabola

This assumption of parabolic profile does not rely on any physical consideration but corresponds to the meniscus shape observed experimentally. The equation of this parabola is given by:

$$r_p(z) = a_0 + a_1 z + a_2 z^2 \tag{2.28}$$

where r and z are the axis shown in Fig. 2.15. The geometric conditions on the parabola are:

1. the symmetry with the r-axis imposes the vertex to be at $z = 0$,
2. the slope at $z = \frac{h}{2}$ is given by the contact angle,
3. the radius at $z = \frac{h}{2}$ is R.

Therefore

$$\begin{aligned} a_1 &= 0 \\ a_2 h &= \cot\theta \\ a_0 + a_2 \frac{h^2}{4} &= R \end{aligned}$$

The parabola is:

$$r_p(z) = R - \frac{h\cot\theta}{4} + \frac{\cot\theta}{h} z^2 \tag{2.29}$$

Since the parabola represents a meniscus, $r_p(z)$ must be positive. The condition for its existence is then:

$$R > \frac{h\cot\theta}{4} \tag{2.30}$$

The volume is:

$$\begin{aligned} V_p &= \pi \int_{-\frac{h}{2}}^{\frac{h}{2}} r_p^2(z) dz \\ &= \pi R^2 h - \frac{\pi R h^2 \cot\theta}{3} + \frac{\pi h^3 \cot^2\theta}{30} \end{aligned} \tag{2.31}$$

The relation between the volume and the contact angle can be inverted. The volume can be considered as an input parameter instead of the contact angle. The local curvature computed from (2.24) is:

$$2H(z) = 2h^2 \frac{2h^2 - 4Rh\cot\theta + h^2\cot^2\theta + 4\cot^2\theta\, z^2}{(4Rh - h^2\cot\theta + 4\cot\theta\, z^2)(h^2 + 4\cot^2\theta\, z^2)^{\frac{3}{2}}} \tag{2.32}$$

The curvatures at the apex (subscript $_0$) and at the triple line (subscript $_3$) are:

$$2H_0 = -\frac{2\cot\theta}{h} + \frac{4}{4R - h\cot\theta} \tag{2.33}$$

$$2H_3 = \sin\theta \frac{h - 2R\sin\theta\cos\theta}{hR} \tag{2.34}$$

From this volume equation, we can determine a_2 and its derivative with respect to h (V is assumed to be constant), consequently, the force F_z can be determined from its both components :

$$\begin{aligned} F_z &= F_L + F_T \\ &= -\pi\gamma R^2 2H_0 + 2\pi\gamma R\sin\theta \end{aligned} \tag{2.35}$$

In the particular case of $\theta = \frac{\pi}{2}$ (corresponding to a cylindrical meniscus), the force is equal to the well-known value $-\pi R\gamma$ (2.7).

The model validation has been performed by comparing the parabolic model output with the force benchmark $F = -\pi R\gamma$ for a cylindrical meniscus and by comparing it with numerical results obtained with Surface Evolver. This has been done for a pad of radius $R = 100\,\mu\text{m}$, a surface tension $\gamma = 72\,\text{mNm}^{-1}$ and a volume of liquid $V = \pi 10^{-12}\,\text{m}^{-3} = \pi\,\text{nL}$, which corresponds to a separation distance between the pad and the component equal to $h_0 = 100\,\mu\text{m}$ for a cylindrical cylinder.

We see in Fig. 2.16 the good correspondence between the parabolic model and the software results, for a large range of separation distances, between 80 and 150 % of the separation distance h_0.

As a conclusion, this analytical model can be used to compute the axial force and the axial stiffness of a liquid meniscus between two circular pads. The validity

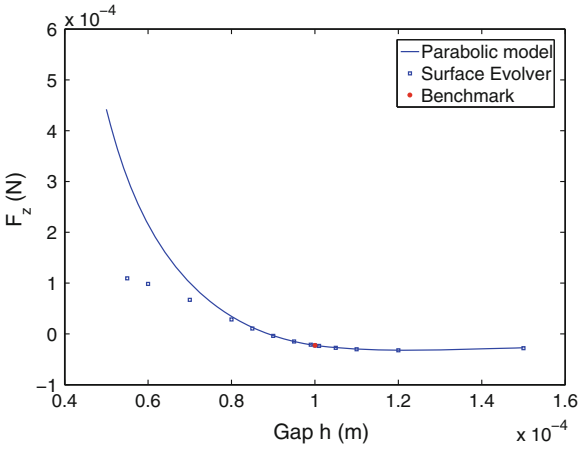

Fig. 2.16 Benchmarking of the force with our parabola model (2.35) with (2.7) and numerical simulation (surface evolver)

domain of this model—deduced from the comparison with numerical results output by Surface Evolver—ranges from 80 to 150 % of the separation distance h_0 for which the meniscus is a cylindre. Let us well note that the lower limit of the physics seems to be about 55 % of h_0. Below this level, the Surface Evolver does not converge anymore, which is related to the non physical existence of such a meniscus.

2.3.2.2 Circular Model

This model assumes a circular profile of the interface shape in the plane rz, of centre (r_c, z_c) and radius ρ (see Fig. 2.17):

$$(r_c(z) - r_0)^2 + (z - z_0)^2 = \rho^2 \tag{2.36}$$

The conditions on the arc of circle are:

1. the symmetry with the r-axis imposes the centre of circle to be on the r-axis,
2. the slope at $z = \frac{h}{2}$ is given by the contact angle,
3. the radius at $z = \frac{h}{2}$ is R.

The symmetry imposes $z_0 = 0$. By differentiating the expression with respect to z, we have:

$$2(r - r_0)\frac{\mathrm{d}r_c}{\mathrm{d}z} + 2z = 0$$

With the above relation, the contact angle can be imposed through the derivative of r_c. With the conditions at $z = \frac{h}{2}$, the position of the centre is:

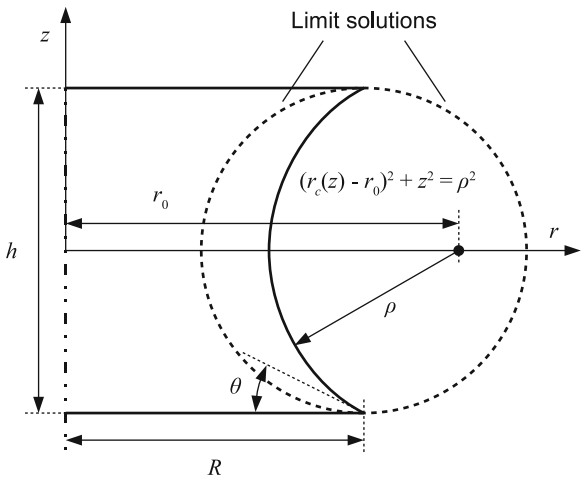

Fig. 2.17 Circular model: as usual, three information (pinned contact angle, pad radius and gap) are used to determine the three coefficients of a parabola

$$r_0 = R + \frac{h}{2}\tan\theta \tag{2.37}$$

Using the third condition:

$$\rho = \frac{h}{2|\cos\theta|} \tag{2.38}$$

With the above conditions, 2.36 may be rewritten under an explicit form $r(z)$. However, the sign of the square root differs when the contact angle is lower or higher than $\frac{\pi}{2}$:

$$r_c(z) = -\sqrt{\frac{h^2}{4\cos^2\theta} - z^2} + R + \frac{h}{2}\tan\theta \qquad \text{if } \theta < \frac{\pi}{2}$$

$$r_c(z) = +\sqrt{\frac{h^2}{4\cos^2\theta} - z^2} + R + \frac{h}{2}\tan\theta \qquad \text{if } \theta > \frac{\pi}{2}$$

More conveniently, by extracting the $\cos\theta$ from the square root, the two relations become:

$$r_c(z) = \frac{-1}{2\cos\theta}\sqrt{h^2 - 4\cos^2\theta\, z^2} + R + \frac{h}{2}\tan\theta \tag{2.39}$$

The reader will notice the singularity at $\theta = \frac{\pi}{2}$: when $\theta = 0$, the centre is at $r = R$. When θ increases, the centre moves towards $+\infty$ (occurring for $\theta = \frac{\pi}{2}$). When $\theta = \pi$, the centre is at $r = R$. The centre moves towards $-\infty$ when θ decreases. The jump of θ from $\frac{\pi}{2} - \varepsilon$ to $\frac{\pi}{2} + \varepsilon$ is accompanied of an abrupt change of the centre of circle from $+\infty$ to $-\infty$. The relation still converges to R when $\theta \to \frac{\pi}{2}$ since:

$$\lim_{\theta \to \frac{\pi}{2}} \left(\tan\theta - \frac{1}{\cos\theta}\right) = 0$$

The volume is:

$$\begin{aligned} V_c &= \pi \int_{-\frac{h}{2}}^{\frac{h}{2}} r_c^2(z)dz \\ &= \pi R^2 h + \frac{\pi R h^2 \tan\theta}{2} + \frac{\pi h^3}{4\cos^2\theta} - \frac{\pi h^3}{12} - \frac{\pi h^2}{4\cos^2\theta}\left(\tfrac{\pi}{2} - \theta\right)(2R + h\tan\theta) \end{aligned} \tag{2.40}$$

The reader will remark that the contact angle cannot be expressed as a function of volume as for the parabolic model. The local curvature is:

$$2H(z) = -\frac{2\cos\theta}{h} + \frac{2\cos\theta\sqrt{h^2 - 4\cos^2\theta\, z^2}}{-h\sqrt{h^2 - 4\cos^2\theta\, z^2} + 2Rh\cos\theta + h^2\sin\theta} \tag{2.41}$$

The curvature at the apex and at the triple line are:

$$2H_0 = -\frac{2\cos\theta}{h} + \frac{2\cos\theta}{2R\cos\theta + h\sin\theta - h} \tag{2.42}$$

$$2H_3 = -\frac{2\cos\theta}{h} + \frac{\sin\theta}{R} \tag{2.43}$$

2.3.2.3 Comparison of the Analytic Models for Axial Forces

The circular model is established following the same development presented above. For a symmetric case (the plane containing the neck is a plane of symmetry so that top and bottom contact angles as well as top and bottom radii are equal), the analytical expressions of the shape, the volume and the curvature are given in Table. 2.1. Input parameters are the radius of the solid liquid interface R, the gap h and the contact angle θ. The volume can also be considered as an input parameter (instead of the contact angle for example).

Table 2.1 Analytical expressions from the parabolic model and the circular model

Parabolic model	$\theta \to \frac{\pi}{2}$
$r_p(z) = R - \frac{h\cot\theta}{4} + \frac{\cot\theta}{h}z^2$	$\to R$
$V = \pi R^2 h - \frac{\pi R h^2\cot\theta}{3} + \frac{\pi h^3\cot^2\theta}{30}$	$\to \pi R^2 h$
$\theta(V) = \frac{5\pi R h^2 - \sqrt{30\pi h^3 V_p - 5\pi^2 R^2 h^4}}{\pi h^3}$	
$2H(z) = 2h^2\frac{2h^2 - 4Rh\cot\theta + h^2\cot^2\theta + 4\cot^2\theta\, z^2}{(4Rh - h^2\cot\theta + 4\cot\theta\, z^2)(h^2 + 4\cot^2\theta\, z^2)^{\frac{3}{2}}}$	$\to \frac{1}{R}$
$2H_0 = -\frac{2\cot\theta}{h} + \frac{4}{4R - h\cot\theta}$	$\to \frac{1}{R}$
$2H_3 = \sin\theta\frac{h - 2R\sin\theta\cos\theta}{hR}$	$\to \frac{1}{R}$
Circular model	
$r_c(z) = \frac{-1}{2\cos\theta}\sqrt{h^2 - 4\cos^2\theta\, z^2} + R + \frac{h}{2}\tan\theta$	$\to R$
$V = \pi R^2 h + \frac{\pi R h^2\tan\theta}{2} + \frac{\pi h^3}{4\cos^2\theta} - \frac{\pi h^3}{12} - \frac{\pi h^2}{4\cos^2\theta}(\frac{\pi}{2} - \theta)(2R + h\tan\theta)$	$\to \pi R^2 h$
$\theta(V)$ = No analytic solution	
$2H(z) = -\frac{2\cos\theta}{h} + \frac{2\cos\theta\sqrt{h^2 - 4\cos^2\theta\, z^2}}{-h\sqrt{h^2 - 4\cos^2\theta\, z^2} + 2Rh\cos\theta + h^2\sin\theta}$	$\to \frac{1}{R}$
$2H_0 = -\frac{2\cos\theta}{h} + \frac{2\cos\theta}{2R\cos\theta + h\sin\theta - h}$	$\to \frac{1}{R}$
$2H_3 = -\frac{2\cos\theta}{h} + \frac{\sin\theta}{R}$	$\to \frac{1}{R}$

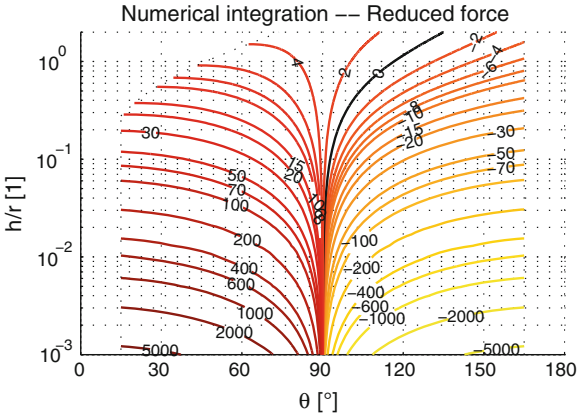

Fig. 2.18 Map of the reduced force $\hat{F} = F/r\gamma$ according to the contact angle θ and the reduced height $\hat{h} = h/r$ computed by numeric integration

The advantages of the parabola model are twofold: switching from negative to positive curvatures is smoothly done when $a_2 = 0$, while the circular approximation is not continuous: the center of the circle abruptly switches from $-\infty$ to $+\infty$ (the mathematical expressions present alocal singularity at $\theta = \frac{\pi}{2}$). Secondly, the volume of liquid can be analytically expressed as indicated by equation, having the advantage to skip the knowledge of the contact angle (contact angles are sometimes difficult to measure).

2.3.2.4 Error Maps for Circular and Parabolic Models

The reduced force $\hat{F} = F/r\gamma$ is represented on a map according to the contact angle θ and the reduced height $\hat{h} = h/r$. On Fig. 2.18, the shape $r(z)$ from 2.24 has been integrated numerically, providing an exact estimation of the curvature and contact angle. The zero force curve does not superpose on the curve $\theta = \frac{\pi}{2}$: the Laplace F_{L} term must cancel the surface tension term F_{T}. At a fixed contact angle θ, the curvature decreases with the reduced gap $\hat{h}$. Therefore when the gap increases, the contact angle must also increase to balance the surface tension force.

To evaluate the accuracy of the analytical approximation of the interface, we present in Fig. 2.19a and b the relative error of the force for both models:

$$\varepsilon_p = \frac{F_p - F}{F} \tag{2.44}$$

$$\varepsilon_c = \frac{F_c - F}{F} \tag{2.45}$$

The parabolic model presents a relative error below 20 % for an angle between 60 and120° (Fig. 2.19a). On the left side of the graph, the error increases near the zero-

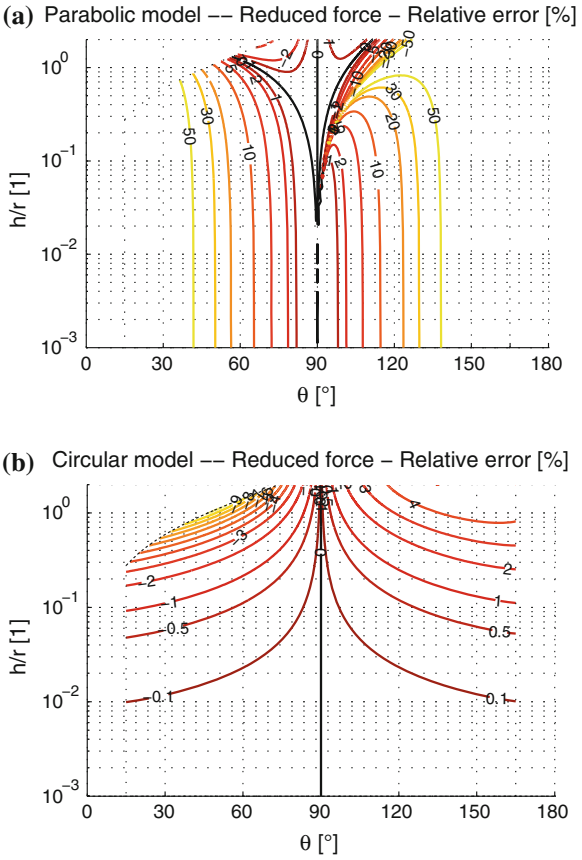

Fig. 2.19 Map of relative error of the reduced force $\hat{F} = F/r\gamma$ according to the contact angle θ and the reduced height $\hat{h} = h/r$

force curve of the exact solution (Fig. 2.18) because there is no perfect match between the parabolic model and the exact solution. Fig. 2.19b shows that the circular model is very accurate, especially at small gap.

2.4 Conclusions

This chapter recalled the fundamentals to calculate capillary forces for simple geometries, either by using the energetic method (Sect. 2.2.1), or by solving the equations exactly (Sect. 2.2.3). Geometrical approximations were also provided, assuming a circular or a parabolic meniscus shape. This preliminary description was limited to equilibrium configurations: axial dynamics will be presented in Chaps. 6, 7.

Acknowledgments This work has been funded by the F.R.I.A.—*Fonds pour la Formation et la Recherche dans l'Industrie et l'Agriculture.*, and developments were achieved among the framework of the European project

Appendix

Capillary Force Developed by a Meniscus at Equilibrium

Let us consider the meniscus depicted in Fig. 2.20. At equilibrium, the sum of forces acting on any slice of the meniscus must be equal to zero. On each face, capillary forces can be split into two contributions: the so-called tension force F_T, due to the action of surface tension along the tangent to liquid-gas interface, and the Laplace or (also called) capillary force F_L originating from the pressure acting on the face.

The force exerted on the bottom face of the slice is equal to:

$$\bar{F}(z) = \left(\underbrace{\pi r^2 \Delta p}_{F_L} - \underbrace{2\pi r \gamma \cos u}_{F_T} \right) \bar{1}_z \tag{2.46}$$

while the force acting on the top face of the slice is given by:

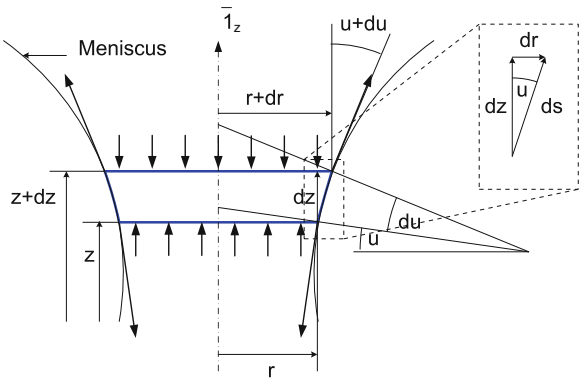

Fig. 2.20 Equilibrium of a meniscus slice comprised between z and $z + dz$. It can be shown that the capillary force computed at height z exactly balance the the capillary force computed at height $z + dz$

$$\begin{aligned}\bar{F}(z+\mathrm{d}z) &= \left(-\pi(r+\mathrm{d}r)^2\Delta p + 2\pi(r+\mathrm{d}r)\gamma\cos(u+\mathrm{d}u)\right)\bar{1}_z \\ &= \left[-\pi r^2\Delta p + 2\pi r\gamma\cos u + 2\pi(\underbrace{-r\mathrm{d}r\Delta p + r\gamma\sin u\mathrm{d}u + \gamma\cos u\mathrm{d}r}_{I})\right]\bar{1}_z\end{aligned} \tag{2.47}$$

The underbraced expression I can be shown to be equal to zero by expressing the Laplace law (Eq. (2.24)):

$$\begin{aligned}\Delta p &= 2H\gamma \\ &= \left(-\frac{r''}{(1+r'^2)^{3/2}} + \frac{1}{r(1+r'^2)^{1/2}}\right)\gamma &(2.48)\\ &= \left(\frac{\mathrm{d}u}{\mathrm{d}s} + \frac{\cos u}{r}\right)\gamma &(2.49)\\ &= \left(\frac{\mathrm{d}u}{\mathrm{d}r}\sin u + \frac{\cos u}{r}\right)\gamma &(2.50)\end{aligned}$$

leading to:

$$I = -r\mathrm{d}u\sin u\gamma - \mathrm{d}r\cos u\gamma + r\gamma\sin u\mathrm{d}u + \gamma\cos u\mathrm{d}r = 0 \tag{2.51}$$

Consequently, the forces $\bar{F}(z) + \bar{F}(z+\mathrm{d}z)$ balance, and the capillary force given by $F(z)$ can be computed at any value of z. This means that in the case of two solids linked by a liquid meniscus, the force can be computed on the top component or on the bottom component. For the sake of convenience, it can also be computed at the neck in case the latter exists (it may not exist if the extremum radius of the meniscus corresponds to one of both wetting radii).

Equivalence of Formulations

A lot of work has been reported on capillary forces modeling (see for example [1, 4–6, 9, 12–14]), based on the energetic method (i.e. derivation of the total interface energy) or a direct force computation from the meniscus geometry, the latter being either determined exactly through the numerical solving of the so-called Laplace equation or approximated by a predefined geometrical profile such as a circle (i.e. toroidal approximation) or a parabola. The energetic approach is usually quite clear on its approximations: the liquid-vapor interface energy is sometimes neglected in order not to compute the exact shape of the meniscus, but an exact solution can be found if the lateral is computed for example by mean of a finite element solver such as Surface Evolver. At the contrary, literature results are not so clear as far as the other method is concerned. For example, some authors neglect the so-called tension term

with respect to the Laplace term . This sometimes pertinent assumption has led many author authors to add the tension term to the result obtained by deriving the interface energy, i.e. to mix both methods. A recent by one of the authors [15] contributed to clarify this situation by showing that the capillary force obtained by deriving the interfacial energy is exactly equal to the sum of the Laplace and tension terms. The equivalence is considered with three qualitative arguments, and an analytical argument is developed in the case of the interaction between a prism and a place. Experimental results also contributed to show this equivalence.

Mathematically, the equivalence between the energetic approach and the direct formulation based on the Laplace and the tension terms can be shown:

$$F = F_{\mathrm{L}} + F_{\mathrm{T}} = -\frac{\mathrm{d}W}{\mathrm{d}z} \tag{2.52}$$

where F_{L} and F_{T} are given by (2.46), W by (2.1). z is the separation distance between both solids.

As it is shown that both approaches are equivalent, it means that the energetic approach already involves the tension term and the Laplace term on an implicit way. Consequently, the energetic approach as proposed by Israelachvili (see (2.8)) includes both terms, even if, for zero separation distance, the pressure term usually dominates the tension one. For axially symmetric configurations, the method based on the Laplace equation will be preferred because it can be easily numerically solved.

References

1. P. Lambert, A. Delchambre, Parameters ruling capillary forces at the submillimetric scale. Langmuir **21**, 9537–9543 (2005)
2. P. Lambert, M. Mastrangeli, J.-B. Valsamis, G. Degrez, Spectral analysis and experimental study of lateral capillary dynamics (for flip-chip applications). Microfluid. Nanofluid. (Published online) (2010)
3. P. Lambert, *Capillary Forces in Microassembly: Modeling, Simulation, Experiments, and Case Study. Microtechnology and MEMS* (Springer, Boston, 2007)
4. J.N. Israelachvili, *Intermolecular and Surface Forces*, 2nd edn. (Academic Press, San Diego, 1992)
5. F.M. Orr, L.E. Scriven, A.P. Rivas, Pendular rings between solids: meniscus properties and capillary force. J. Fluid Mech. **67**, 723–742 (1975)
6. Yakov I. Rabinovich, Madhavan S. Esayanur, Brij M. Mougdil, Capillary forces between two spheres with a fixed volume liquid bridge: theory and experiment. Langmuir **21**, 10992–10997 (2005)
7. A. Chau, S. Régnier, A. Delchambre, P. Lambert, Theoretical and experimental study of the influence of AFM tip geometry and orientation on capillary force. J. Adhes. Sci. Technl. **24**, 2499–2510 (2010)
8. P.-S. de Laplace, Sur l'action capillaire, in *Mécanique Céleste—Supplément au Livre X*, pp. 349–498, Courcier, Paris (1805)
9. A. de Lazzer, M. Dreyer, H.J. Rath, Particle-surface capillary forces. Langmuir **15**(13), 4551–4559 (1999)

10. P. Lambert, P. Letier, A. Delchambre, Capillary and surface tension forces in the manipulation of small parts, in *Proceedings of International Symposium on Assembly and Tasks Planning (ISATP)*, pp. 54–59 (2003)
11. J.-B. Valsamis, A study of liquid bridges dynamics: an application to micro-assembly. Ph.D. thesis, Université libre de Bruxelles
12. X. Pepin, D. Rossetti, S.M. Iveson, S.J.R. Simons, Modeling the evolution and rupture of pendular liquid bridges in the presence of large wetting hysteresis. J. Colloid Interface Sci. **232**, 289–297 (2000)
13. Y.I. Rabinovich, J.J. Adler, M.S. Esayanur, A. Ata, R.K. Singh, B.M. Mougdil, Capillary forces between surfaces with nanoscale roughness. Adv. Colloid Interface Sci. **96**, 213–230 (2002)
14. T. Stifter, O. Marti, B. Bhushan, Theoretical investigation of the distance dependence of capillary and van der Waals forces in scanning force microscopy. Phys. Rev. B **62**(20), 13667–13673 (2000)
15. P. Lambert, A. Chau, A. Delchambre, S. Régnier, Comparison between two capillary forces models. Langmuir **24**(7), 3157 (2008)

http://www.springer.com/978-3-642-37551-4

Surface Tension in Microsystems
Engineering Below the Capillary Length
Lambert, P. (Ed.)
2013, XXIX, 327 p. 174 illus., 42 illus. in color.,
Hardcover
ISBN: 978-3-642-37551-4